Research Square

Preprints are preliminary reports that have not undergone peer review.
They should not be considered conclusive, used to inform clinical practice,
or referenced by the media as validated information.

Fluorescent Indolo[2,3-b]quinoxalin-2-yl) (Phenyl)methanone Dyes: Photophysical, Aie Activity, Electrochemical, and Theoretical Studies

Deepali Kanekar
University of Mumbai Faculty of Science
Sudhakar Dhanawade
University of Mumbai Faculty of Science
Anand Jadhav
University of Mumbai Faculty of Science
Mohmmed Ghadiyali
University of Mumbai Faculty of Science
Sajeev Chacko
University of Mumbai Faculty of Science
Rajesh M Kamble (kamblerm@chem.mu.ac.in)
University of Mumbai https://orcid.org/0000-0001-9059-249X

Research Article

Keywords: Indolo[2,3-b]quinoxalin-2-yl)(phenyl)methanone derivatives, Donor–Acceptor (D–A) architecture, Intramolecular charge transfer (ICT) transitions, Aggregation-Induced Emission (AIE) effect, HOMO and LUMO energy levels, n-type/electron transporting materials

Posted Date: December 29th, 2021

DOI: https://doi.org/10.21203/rs.3.rs-1195228/v1

License: This work is licensed under a Creative Commons Attribution 4.0 International License. Read Full License

Abstract

Herein, we have synthesized four indolo[2,3-*b*]quinoxalin-2-yl)(phenyl)methanone derivatives **1**–**4** by cyclocondensation. The photophysical studies of dyes in various solvents and neat solid film exhibit typical electronic spectra with inbuilt intramolecular charge transfer (ICT) (λ_{max}: 397–490 nm) confirming donor-acceptor architecture. Herein, dyes fluoresce in the blue-orange region (λ_{Emax}: 435–614) on excitation at their ICT maxima in toluene, ethyl acetate, chloroform, DMSO, and neat solid film. **1** and **2** which exhibit good emission intensity in all mediums, were studied for aggregation-induced emission (AIE) effect. Electrochemical studies indicate **1**–**4** possess relatively low lying LUMO (−3.65 to −3.98 eV) comparable to reported n-type/electron-transporting materials. The HOMO and LUMO energy levels in **1**–**4** were evaluated by DFT and TD-DFT calculations. TGA analysis shows **1**–**4** exhibit good thermal stability. The characteristic optoelectronic properties and thermal stability signify these dyes are potential candidate for their application in optoelectronics.

Introduction

Organic materials are emerging as third-generation materials due to their widespread applications in organic light-emitting diodes (OLEDs) [1,2], organic field-effect transistors (OFETs) [3], dye-sensitized solar cells (DSSCs) [4–6], non-linear optics (NLO's) [7], chemo /biosensors [8,9], etc. Researchers are making effort to further improve the efficiency and lifetime of organic materials, to exploit their hidden potential. As organic materials offer low cost and easy device fabrications. In particular, the donor-acceptor (D–A) based design approach which enables simpler tuning of optoelectronic properties with molecular engineering, was found to be promising to obtain organic material with diverse properties such as solvatofluorochromism, two-photon excited fluorescence, triplet-triplet annihilation (TTA), thermally activated delayed fluorescence (TADF), and charge transport (hole/electron). However, the fluorescence of many organic fluorophores which emit brightly in solution state get diminishes in solid/aggregate state due to aggregation-caused quenching (ACQ). Indeed, it is desirable to have molecules emit in a solid/aggregate state for their real-world application. In 2001, Tang *et.al.* first introduced aggregation-induced emission (AIE) which is contradictory to detrimental ACQ [10]. The twist in molecular structure, attachment of bulky donor groups or incorporation of AIEgens (eg. Tetraphenylethene (TPE), hexylphenylsilole (HPS)) to ACQ fluorophores (anthracene, pyrene, PBI, BODIPY, TPA, carbazole, etc) can be an effective approach to obtain AIE active molecules [11,12].

Additionally, the charge transport in an organic molecule is very important to realize for their application in devices. Organic materials should have HOMO/LUMO energy levels comparable to the work function of commonly used electrodes (Anode: ITO and Cathode: Ca/Al/Mg) to facilitate charge transport [13]. Organic semiconducting molecules which have HOMO(LUMO) levels at around 5.0(4.0) eV are capable of hole(electron) transport and known as hole(electron)-transporting or p(n)-type materials [14,15]. Compared to p-type, the development of n-type materials has lagged due to their difficult synthesis and instability under ambient conditions (in presence of H_2O/O_2). This raise the need of air-stable n-type materials as it is an integral part of the complementary circuit and received unprecedented attention from researchers. Though there is no general guideline to obtain air-stable n-type materials, according to the literature LUMO level can be lowered through the introduction of electron-withdrawing groups –F, –CN, –Cl, $-NO_2$, –COOH, $-CF_3$ and

perfluorinated alkyl chain in p-type materials; An alternative approach is the incorporation of electronegative heteroatoms like **N** or **S** to acceptor core of D-A system can promote injection and transport of electrons in resulting molecules [16]. Previously, we designed and reported different D-A based molecules comprised of donor moieties like aromatic amines (triarylamine/diarylamine/ aryl), heterocyclic amine (carbazole/phenothiazine), and acceptor moieties quinoxaline [17–21], indoloquinoxaline [22,23], phenazine [24-26], pyrido-pyrazine [27,28], pyrazino-phenazines [29] acridone [30], and anthraquinone [31], to obtain a broad range of emission, solvatofluorochromism, AIE, TADF, hole/electron/bipolar charge transport for their application in organic electronics.

Indoloquinoxaline (IQ) is also one of the important classes of N-containing heterocyclic compounds. Compared to organic electronics, indole and its IQ derivatives have been extensively studied in bio/medical chemistry for two reasons (i) as it shows the wide spectrum of biological activity such as anti-viral [32,33], anti-cancer [34,35], anti-microbial [36], anti-bacterial agents [37], anti-HIV and so on [38]. (ii) indole is a chromophore of important amino acid, tryptophan [39]. Along with the importance of luminescence of indole in tryptophan, literature also witnesses complexity in emission spectra of indole derivatives in various solvents due to the presence of two degenerate excited states L_a and L_b differing in dipole moment demonstrating sensitivity towards solvent polarity [39–41].

Encouraged by previous work, and looking at the scope of IQ materials in organic electronics, we present the design and synthesis of four indolo-quinoxaline (IQ) derivatives, based on inbuilt D-A architecture in which electron-rich indole act as a donor and electron-deficient quinoxaline act as an acceptor. Further, the electron deficiency of quinoxaline has been increased through the introduction of the benzoyl segment. The presence of the benzoyl group is not only useful to lower the LUMO level but also responsible to bring some twist in the molecule so that detrimental π-π stacking in solid-state get minimized. The influence of electron-donating ($-CH_3$) and withdrawing substituents ($-Br$, $-NO_2$) and increased electron deficiency of acceptor core through benzoyl unit, on opto-electrochemical properties have been studied. The detailed photophysical, AIE, electrochemical, thermal, and theoretical properties of synthesized dyes are investigated. The molecular structure of IQ derivatives is presented in **Figure 1**.

Experimental Section

Chemicals and materials

All the starting materials and reagents were purchased from commercial sources (Sigma Aldrich and Alfa Aesar) and were used without any further treatment and purification unless otherwise mentioned. The organic solvents were of HPLC and spectroscopic grade and were dried and freshly distilled using the standard procedures and handled in a moisture-free atmosphere. Column chromatography was carried out using SD-fine silica gel (60–120 mesh), eluting with n-hexane and chloroform. The progress of the reaction and the purity of the compound was checked by thin-layer chromatography (TLC) on silica-gel-coated glass plates, in which the spots were visualized with UV light (365 nm) and in an iodine chamber.

Instrumentation and methods

UV-visible spectra were recorded in 10^{-6} mol L^{-1} solution in a 1 cm path length quartz cuvette as well as the neat solid films on a SHIMADZU UV-2401PC instrument at room temperature. The neat solid films of compounds **1**–**4** were prepared by using a spin coater (Holmarc HO-TH-05) at 1000 rpm for 2 min ~6 mg mL^{-1} of the sample in chloroform. Quartz plates were used for neat solid film studies. The excitation and emission spectra were carried out on a Perkin Elmer LS 55 Fluorescence spectrophotometer. Cyclic voltammetry studies were carried out on a computer-controlled Palmsens3 potentiostat. Typically, a three-electrode cell equipped with a glassy carbon working electrode, an Ag/AgCl (non-aqueous) reference electrode, and platinum (Pt) wire as the counter electrode was employed. The measurements were carried at room temperature in anhydrous dichloromethane with tetra-butyl ammonium hexafluorophosphate solution (0.1 M) as the supporting electrolyte with a scan rate of 100 mVs^{-1}. The potential of the Ag/AgCl reference electrode was calibrated by using a ferrocene/ferrocenium redox couple, which has a known oxidation potential of +5.1 eV. The thermogravimetric analysis (TGA) was performed using a Mettler Toledo instrument (TG) under nitrogen atmosphere. ^{1}H and ^{13}C NMR spectra were recorded using $CDCl_3$ on Varian 300 MHz Ultra shield spectrometer with tetramethylsilane (TMS) as an internal reference at working frequency 300 MHz and 75 MHz respectively. Fourier transform infrared (FT–IR) spectra were recorded on a Perkin Elmer Frontier 91579. Mass spectrometric measurements were recorded using MALDI–TOF (Bruker) and elemental analysis was carried out on EA Euro–elemental analysis instrument. To confirm the formation of nanoparticles in AIE studies, the sample of synthesized dye was analysed by Dynamic light scattering (DLS) technique using Zetasizer Ver. 7.12, serial number: MAL1180779.

Synthesis Procedures

Methylation of isatin and its derivatives:

To increase the solubility of isatin and its $-CH_3$, –Br, and $-NO_2$ derivatives, N-methylation was done according to a reported procedure by Beauchard et al [42].

General method for the synthesis of compound 1–4:

The synthetic method given by Bergman et.al have been used for the preparation of **1**–**4**, wherein a mixture of 3,4-diaminobenzophenone (1.0 mmol) and 5-Substituted-1-methyl-1*H*-Indole-2,3-dione (1.2 mmol) were dissolved in glacial acetic acid (10 ml) and refluxed for 3–4 hours [43]. The reaction mixture was cooled to room temperature and neutralized with sodium hydrogen carbonate to pH 7. The resulting solid obtained by vacuum filtration was washed thoroughly with H_2O and kept for air-drying overnight. The crude product obtained was further purified with different ratios of n-hexane/chloroform by silica gel column chromatography to obtain Yellow to orange solid. (Compound **1**, **2**, **3**, and **4** were purified by using n-hexane/chloroform with ratio 90:10, 90:10, 80:20, and 70:30 respectively).

(6-methyl-6*H*-indolo[2,3-*b*]quinoxalin-2-yl)(phenyl)methanone (**1**)

Yellow solid; 286 mg (84%); mp 261 °C. FT–IR (KBr, λ_{max} cm^{-1}): 3050, 2919, 1710, 1650, 1583, 1257,1200, 752; ^{1}H NMR (300 MHz, $CDCl_3$): δ 8.82 – 8.03 (m, 4H), 8.01 – 7.79 (m, 2H), 7.76 – 7.30 (m, 6H), 3.94 (s, 3H)

(–NCH_3); ^{13}C NMR (75 MHz, $CDCl_3$): δ 196.27 (C=O), 145.47, 141.61, 141.07, 139.48, 137.09, 134.49, 132.54, 131.85, 137.10, 131.15, 130.17, 129.69, 128.83, 128.43, 125.93, 122.81, 121.81, 121.53, 121.33, 119.08, 109.39, 27.66 (–NCH_3); MALDI-TOF: mass calcd for $C_{22}H_{15}N_3O$ [M^+]: 337.12 found: 337.90; elemental anal. calcd for $C_{22}H_{15}N_3O$: C 78.32, H 4.48, N 12.46 found: C 78.18, H 4.38, N 12.52.

(6,9-dimethyl-6*H*-indolo[2,3-*b*]quinoxalin-2-yl)(phenyl)methanone (**2**)

Yellow solid; 273 mg (81%); mp 278 °C. FT–IR (KBr, λ_{max} cm^{-1}): 3057, 2918, 2861, 1707, 1651, 1570, 1487, 1280, 1117, 803, 718; ^{1}H NMR (300 MHz, $CDCl_3$): δ 8.52–8.08 (m, 4H), 8.00–7.80 (m, 2H), 7.71–7.28 (m, 5H), 3.91 (s, 3H) (–NCH_3), 2.56 (s, 3H) (–CCH_3); ^{13}C NMR (75 MHz, $CDCl_3$): δ 196.34 (C=O), 143.70, 141.05, 139.46, 136.96, 133.36, 133.05, 132.71, 132.52, 132.33, 131.14, 130.99, 130.17, 129.67, 128.53, 128.05, 125.86, 123.04, 122.70, 119.16, 109.12, 27.58 (–NCH_3), 21.29 (–CCH_3); (MALDI-TOF: mass calcd for $C_{23}H_{17}N_3O$ [M^+]: 351.41 found: 351.97; elemental anal. calcd for $C_{23}H_{17}N_3O$: C, 78.61; H, 4.88; N, 11.96; found: C 78.71, H 5.03, N 11.89.

(9-bromo-6-methyl-6*H*-indolo[2,3-*b*]quinoxalin-2-yl)(phenyl)methanone (**3**)

Brown solid; 262 mg (78%); mp 290 °C. FT–IR (KBr, λ_{max} cm^{-1}): 3061, 2927, 2861, 1706, 1651, 1564, 1443, 1279, 1117, 803, 718; ^{1}H NMR (300 MHz, $CDCl_3$): δ 8.70–8.48 (m, 2H), 8.45–8.11 (m, 2H), 8.03–7.74 (m, 3H), 7.73–7.49 (m, 3H), 7.37 (d, *J* = 8.6 Hz, 1H), 3.95 (s, 3H) (–NCH_3); ^{13}C NMR (75 MHz, $CDCl_3$): δ 196.06 (C=O), 143.94, 143.77, 140.35, 139.94, 134.09, 132.49, 132.14, 131.14, 130.19, 130.09, 130.06, 129.30, 128.58, 128.47, 128.31, 126.28, 126.24, 125.77, 122.70, 114.01, 110.98, 27.57 (–NCH_3); MALDI-TOF: mass calcd for $C_{22}H_{14}BrN_3O$ [M^+]: 416.28 found: 416.51, [M+2]: 418.43; elemental anal. calcd for $C_{22}H_{14}BrN_3O$: C, 63.48; H, 3.39; N, 10.09 found C, 63.37; H, 3.46; N, 9.98.

(**6-methyl-9-nitro-6*H*-indolo[2,3-*b*]quinoxalin-2-yl)(phenyl)methanone** (**4**)

Orange solid; 134 mg (40%); mp >300 °C. FT–IR (KBr, λ_{max} cm^{-1}): 3063, 2918, 2849, 1719, 1651, 1582, 1502, 1487, 1320, 1117, 797, 709; ^{1}H NMR (300 MHz, $CDCl_3$): δ 8.72–8.47 (m, 2H), 8.42–8.27 (m, 1H), 8.25–8.12 (m, 1H), 8.05–7.77 (m, 3H), 7.70–7.46 (m, 3H), 7.43–7.33 (m, 1H), 3.97 (s, 3H) (–NCH_3); ^{13}C NMR could not obtained due to poor solubility; MALDI-TOF: mass calcd for $C_{22}H_{14}N_4O_3$ [M^+]: 382.11 found: 382.28; elemental anal. calcd for $C_{22}H_{14}N_4O_3$: C, 69.10; H, 3.69; N, 14.65 found C, 69.14; H, 3.58; N, 14.81.

Results And Discussion

Synthesis and Characterization

Four indolo[2,3-*b*]quinoxalin-2-yl)(phenyl)methanone derivatives based on D–A architecture have been synthesized through simple cyclo-condensation reaction, The synthesis of target compounds is shown in **Scheme 1**. IQ derivatives **1–4** were synthesized in two steps. Firstly, isatin derivatives were alkylated at their N–position to increase the solubility of the target molecules, and later these N–methylated isatin derivatives

were reacted with 1,2-diaminobenzophenone in acetic acid for 3–4 hours to produce desired cyclo-condensed product **1–4**. The four target compounds were obtained in good yield (40–85%) as yellow-brown solids. The identity and purity of all new compounds were confirmed by several characterization methods such as FT-IR, ^{1}H–NMR, ^{13}C–NMR, MALDI–TOF, etc. The inbuilt D–A architecture and HOMO-LUMO orbital energies were further rationalized using DFT calculations.

Photophysical Properties

First, photophysical properties of **1–4** were studied in increasing polarity of solvents *viz*., toluene, ethyl acetate, chloroform, and DMSO to understand the effects of solvent polarity on spectral profiles of dyes and have correlated it with their structures. The pertinent data are listed in **Table 1** and absorption spectra of **1–4** recorded in solution are presented in **Figure 2**.

The absorption spectra of **1–4** in different solvents, dominated by multiple overlapping bands assigned to different chromophoric segments in the molecule where, the intense bands in the region 261–404 nm corresponds to high energy n–π* and π–π* transitions in the molecules. The characteristic dual absorptions band between 324–369 nm suggests the occurrence of π–π* transitions from S_0 to S_2 and S_1 state, respectively which could arise from the indole segment of the molecule [44]. Additionally, all derivatives exhibit lower energy transition around 397–490 nm that can be assigned to inbuilt intramolecular charge transfer (ICT) from electron-donating indole unit to electron-deficient quinoxaline core. These ICT transitions were bathochromically shifted for derivatives **2–4** substituted with electron-donating/withdrawing group compared to **1**.

Table 1: UV-vis and Photoluminescence (PL) spectroscopic parameters of **1–4** in solution and neat solid film.

Compound[a]	Medium	UV-vis		PL		Stoke's shift, (cm^{-1})[e]
		λ_{max} (nm) ($\log \varepsilon_{max}$)[b]	(E_g^{opt}, eV)[c]	λ_{em} (nm)	(ϕ_F)[d]	
1	Toluene	347 (5.01), 362 (5.04), 408 (4.38)	2.70	480	0.23	3676
	EA	279 (5.36), 295 (5.26), 361 (5.03), 346 (5.01), 408 (4.32)	2.69	494	0.17	4266
	$CHCl_3$	280 (5.39), 347 (4.86), 364 (4.89), 415 (4.32)	2.62	486	0.16	3520
	DMSO	281 (5.10), 351 (4.49), 365 (4.67), 414 (4.00)	2.61	439*	–	–
	FILM	280, 368, 423	-	515, 537	–	4223, 5018
2	Toluene	350 (4.90), 367 (4.97), 412 (4.40)	2.57	458, 482	0.18	2437, 3524
	EA	282 (5.45), 349 (4.90), 365 (4.97), 414 (4.17)	2.64	525	0.09	5106
	$CHCl_3$	284 (5.33), 353 (4.85), 369 (4.91), 420 (4.34)	2.56	443, 527	0.12	1236, 4834
	DMSO	282 (5.10), 354 (4.49), 368 (5.35), 423 (3.78)	2.52	440*	–	–
	FILM	282, 330, 457	-	537	–	3259
3	Toluene	348 (4.92), 362 (4.93), 404 (4.60), 489 (4.32)	2.08	435, 460	0.11	–2538, –1289
	EA	261 (5.32), 286 (5.40), 346 (4.93), 362 (4.97), 417 (4.34), 475 (4.23)	2.25	559	<0.01	3163
	$CHCl_3$	286 (5.39), 350 (4.95), 366 (4.99), 490 (4.32)	2.23	582	0.07	3226
	DMSO	268 (4.84), 286 (4.88), 352 (4.44), 366 (4.49), 432 (3.85)	2.25	NA	–	–
	FILM	296, 367, 510	-	614	–	3321
4	Toluene	324 (5.10), 356 (5.10), 450 (4.78)	2.37	508	0.01	2537
	EA	281 (5.10), 357 (5.13), 413 (4.34), 445 (5.83)	2.44	NA	–	–
	$CHCl_3$	281 (5.45), 361 (5.16), 444 (4.87)	2.46	544	0.09	9364
	DMSO	263 (4.86), 281 (4.87), 360 (4.68), 397 (3.70)	2.48	451*	–	–
	FILM	371, 501	-	556	–	1974

[a]Recorded in 10^{-6} M solution; [b]log ε_{max} molar absorptivity in solution ($M^{-1}cm^{-1}$)

[c]Optical band gap estimated using offset wavelength derived from the low energy absorption band $\left(E_g^{opt} = \frac{1240}{\lambda_{abs\ edge}}\right) eV$

[d]Quantum yield with reference to fluorescein (ϕ = 0.79 in 0.1 M NaOH); [e]Stoke's shift calculated according to the equation $\Delta\nu = (1/\lambda_{abs} - 1/\lambda_{em}) \times 10^7$ (cm^{-1});

NA: Quenched Emission; *featureless emission

The ICT band in **3** is most red-shifted with 18–81 nm and covers a broad range (up to 600 nm) suggests an increased electron-donating strength of indole due to –Br substituent (**+M** mesomeric effect). Besides this, high-intensity ICT transitions in **4** indicate better charge separation and charge transfer in the D-A system due to the presence of electron-withdrawing $-NO_2$ (**–I** inductive effect) on indole moiety. Dyes display good molar absorptivity and almost similar absorption spectra with varying intensities in different solvents. The longer wavelength ICT band seems slightly sensitive towards the nature of solvents. The optical band gap of compounds estimated from the offset wavelength of the low energy absorption band lies within the range 2.08–2.70 eV in solution (**Table 1**). Thereafter, in the neat solid film the absorption spectra of **1**–**4** (**Figure 4a**) displayed broadening of bands with a significant redshift of 8–104 nm in absorption maxima attributed to the molecular aggregation.

The other photophysical data such as optical band gap, emission data, Stoke's shift, and quantum yield were also calculated and summarized in **Table 1**. Dyes **1**–**4** emits blue-orange fluorescence with emission maxima λ_{Emax}: 458–614 nm on excitation at their respective ICT maxima in toluene, ethyl acetate, chloroform, DMSO, and neat solid film. (**Figure 3** and **4** (**A**)). The quantum yield of **1**–**4** was calculated using fluorescein (Φ = 0.79 in 0.1 N NaOH) as a reference and are in the range 0.01–0.23 in toluene.

Dye **1** and **2** display detectable emissions in toluene, ethyl acetate, and chloroform whereas weak emissions obtained for dye **3** and **4** in toluene get considerably quenched in more polar solvents except in chloroform. This reduced intensity or quenching of emission might be due to the presence of –Br in **3** and strong electron-withdrawing $-NO_2$ in **4**.

On contrary, the ability of H-bonding bonding by –Br and $-NO_2$ group present in **3** and **4** with chloroform is responsible for improved long-wavelength emission at λ_{Emax}: 582 nm and λ_{Emax}: 544 nm respectively. Further, all dyes in more polar solvent DMSO displays quenching in emission with featureless emission spectra indicating the occurrence of non-radiative relaxation of the excited state through dipole-dipole interaction. Intriguingly, the bathochromic shift in the emission of dyes with the decrease in emission intensity from toluene (non-polar) (λ_{Emax}: 435–508 nm) to chloroform (λ_{Emax}: 443–582 nm) and quenching of emission in polar DMSO demonstrate the sensitivity of dyes towards polarity of the solvent. (See Supporting information (**SI**), **Figure S1,** for the enlarged emission spectra in above-mentioned solvents)

Nonetheless, emission maxima in the different solvent, ICT absorption band, and Stoke's shift of dyes in solution suggests the existence of specific solute-solvent interaction [45]. In toluene, derivative **3** emits at a shorter wavelength (λ_{Emax}: 435, 460 nm) compared to ICT absorbance maxima (λ_{ICTmax}:489 nm). Though

the emission intensity is low, the observed shorter wavelength emission and longer wavelength-broad ICT absorbance band with anti-Stoke's shift in **3** is probably the consequence of the occurrence of hot-band absorption or some up-conversion process in a molecule. In hot-band absorption, the molecule absorbs from a higher vibrational level (hot band) of the ground state thus results in a longer wavelength (lower energy) absorbance band and emission obtained is the usual fluorescence process that gives anti-Stoke's shift. However, in the up-conversion process, the excited state ion absorbs energy from another excited state ion (or sensitizer) and reaches to higher excited state that leads to high energy emission with anti-Stoke's shift. Luminescent materials possessing anti-Stoke's shifts are useful in bio-applications [46].

Furthermore, dye **1** and **2** display more red-shifted emission and greater Stoke's shift in ethyl acetate than chloroform verify specific solute-solvent interaction in ethyl acetate. This specifies more stabilization of the excited state of dye with orientation polarizability of ethyl acetate. Excluding the exception of anti-Stoke's shift observed for dye **3** in toluene, all dyes exhibit considerable Stoke's shift in the range 1236–9364 cm^{-1} in solution and solid film which ensures reduction of reabsorption of the emitted photons.

Almost all dyes exhibit more or less emission in the neat solid film with a bathochromic shift of 12-79 nm compared to the solution. It could be attributed to intermolecular aggregation in the solid state. Dyes **1** and **2** display better emission in solid-state reveals the capability of aggregation induce emission tested for AIE characteristic.

AIE Phenomenon

In order to estimate the presence of AIE properties in dye **1** and **2** at the preliminary stage, we have prepared a series of THF/water mixtures (0–100%) of **1** and **2** according to the reported procedure [47] to form nanoaggregates of organic dyes and observed them under UV-light. The changes in fluorescence properties of dye with varying concentrations of water from 0–100% have been studied thoroughly and presented in **Figure 5** (For AIE of dye **2**, See **SI Figure S2**).

This shows at higher water fractions quenching of luminescence is greatly recovered due to the presence of AIE activity.

Both the dyes exhibit yellow emission in pure THF solution that could be attributed to inbuilt ICT from donor indole unit to acceptor quinoxaline core. Further, the addition of water dramatically decreases the emission intensity of dye solution with the slight redshift from f_w 10% to 80% and up to 70% in **1** and **2** respectively indicate the occurrence of the positive solvatochromism that could be a result of increased solvent polarity due to the addition of water. Thereafter, enhancement of water content onwards f_w 80% in **1** and 70% in **2** greatly recovers the emission of dyes, implying the formation of nanoaggregates at higher water fraction. The formation of nanoaggregates restricts detrimental relaxation processes such as intramolecular rotations (RIR) and vibrations (RIV), open up the radiative channel, and allows luminophore emits strongly [48]. Both the dyes solution depicts the highest luminescence at f_w 95% with the relative intensity of ~ 1016 and ~136 in **1** and **2**, spectacle the presence of aggregation-induced enhanced emission (AIEE) and AIE respectively. This more and less emission intensity of nanosuspensions corresponds to different physical constraints/modes of aggregation, effective electronic conjugation, and yield of nanoparticles [12]. The

difficulty to control the size, shape, and yield of nanoparticle formation at higher water fractions usually results into an irregular pattern of AIE intensity [12,49]. The level off tail or light scattering at higher water fraction mixtures in absorption spectra is due to the formation of nanoaggregates in suspension. This phenomenon is also known as “Mie scattering” [50] (For Absorption Spectra, See **SIFigure S3**). The formation and stability of nanosuspensions were further examined and confirmed by DLS, helped to relate emission intensity with the size and stability of nanosuspensions. The highest emission intensity obtained at f_w 95% for both dyes **1** and **2** is the result of the smallest hydrodynamic size and low polydispersity index (PDI < 0.5) of nanoaggregates. It shows emission intensity is inversely proportional to the hydrodynamic size of nanosuspension and directly proportional to the stability of nanoaggregates.

Electrochemical properties

The electrochemical behaviour of dyes and their energy level were identified by cyclic voltammetry. The experiment was performed in anhydrous dichloromethane with tetrabutylammonium hexafluorophosphate (Bu4NPF6) as electrolyte and ferrocene as an internal standard to calibrate redox potential. The cyclic voltammogram of dye **3** and graph of optical vs electrochemical bandgap of **1**–**4** are presented in **Figure 6** and the pertinent data preserved in **Table 2**. (for CV of other compounds, see **SI Figure S4**).

Table 2. Electrochemical and thermal data of **1**–**4**.

Compd	E_{oxi}^{peak} [a]	E_{red}^{peak} [b]	HOMO[c]	LUMO[d]	E_g[e]	T_d (^{0}C)[f]
1	–	– 0.94, –1.39,	– 6.35	– 3.65	2.70	261 (286)
2	–	– 0.92, –1.36	–6.29	– 3.72	2.57	274 (288)
3	1.31	–0.90, –1.30	–5.64	–3.72	1.92	294 (312)
4	–	–0.64, –0.94, –1.37	–6.28	–3.98	2.30	314 (335)

[a] E_{oxi}^{peak} oxidation peak potential (V). [b] E_{red}^{peak} reduction peak potential (V). [c] HOMO energy level calculated from $E_{HOMO} = -[E_{oxi}^{peak} - E_{redox}(Fc/Fc^+) + 5.1]$ eV for compound **3** or $E_{HOMO} = -[E_g^{opt} - E_{LUMO}]$ eV for compounds **1**, **2** and **4**. [d] LUMO energy level calculated from $E_{LUMO} = -[E_{red}^{peak} - E_{redox}(Fc/Fc^+) + 5.1]$ eV. [e] E_g = [HOMO – LUMO] eV. [f] Decomposition temperature at 5% and 10% (in parentheses) weight loss derived by TGA.

On an anodic sweep, a noticeable irreversible oxidation peak observed in **3** corresponds to the oxidation of indole segment in the molecule, whereas no proper oxidation peak has been detected in **1**, **2,** and **4** due to the low intensity of the oxidation wave. Further, the cathodic sweep of **1**–**4** predominately exhibits two quasireversible waves corresponding to the reduction of quinoxaline unit and carbonyl group in the benzoyl arm of the synthesized molecules. In addition to this, one extra quasireversible reduction peak obtained for derivative **4** can be assigned to the reduction of electron-withdrawing $-NO_2$ group present on indole moiety.

The HOMO and LUMO energy levels of organic materials are the crucial parameters for their application in optoelectronic devices. Thus, to estimate HOMO and LUMO energy levels and to understand the type of

charge transport in the molecules, the LUMO energy level of **1**–**4** was calculated by using the first reduction potential whereas the HOMO level of all dyes except **3** was calculated using the difference of optical band gap and LUMO energy values. The first oxidation potential obtained in the Cyclic Voltammogram of **3** has been used to calculate its HOMO level. The calculated HOMO and LUMO energy values of **1**–**4** falls within the range – 5.64 to –6.35 eV and – 3.65 to –3.98 eV respectively. Among these dyes, $-NO_2$ substituted indoloquinoxaline derivative **4** possesses the lowest LUMO (–3.98 eV) may be due to the increased electron-accepting strength of the electron-withdrawing inductive effect (**–I** effect) of $-NO_2$. Thereafter, –Br substituted derivative **3** shows low LUMO (–3.72 eV) with optimized HOMO (–5.64 eV) compared to unsubstituted derivative **1** indicate the influence of **–I** and mesomeric effect (**+M** effect) of –Br group on the energy level of the molecule. The LUMO energy levels of **1**–**4** is comparable with reported n-type materials perfluoroalkyl substituted C60-fused N-methylpyrrolidine-para-dodecyl phenyl derivative (C60PC12F25) (LUMO = –3.63 eV) [51], N,N'-bis(1*H*,1*H*,2*H*,2*H*-perfluorodecyl)-1,4,5,8-naphthalene tetracarboxylic diimide [52] and Pyromellitic diimide derivatives [53] indicate their capability of electron transport. The electrochemical bandgap of **1**–**4** is in the range of 1.92–2.70 eV and comparable with the optical band gap **(Figure 6**(**b**)).

Theoretical Properties

Quantum chemistry calculations are performed using Gaussian03 within the framework of density functional theory (DFT). The final geometries for each molecule were obtained by optimizing the initial structure in the gas state within the approximation of B3LYP hybrid exchange-correlation functional and 6-311++G** basis set [54]. The optimized structure, electronic distribution in the frontier molecular orbitals, and absorption spectra of **1** in the gas phase and different solvents (toluene, chloroform, and DMSO) are presented in **Figure 7** (for other compounds, see **SI Figure S17–S25**).

Though HOMO and LUMO orbitals of derivatives are overlapped, it can be distinguished that HOMO orbital preside mainly on electron-rich indole and the LUMO orbital strongly resides on accepting moieties like quinoxaline and carbonyl. The location of HOMO(LUMO) orbitals on the indole(quinoxaline) features the inbuilt donor-acceptor architecture in derivatives.

The first ionization potential, electron affinity, HOMO - LUMO levels, bandgap, and ground-state dipole moment were computed for the dyes **1**–**4** and given in **Table 3.** The HOMO(LUMO) energy of **1**–**4** is in the range of –6.05 to –6.70 eV (–2.50 to –2.99 eV), which are comparable with the experimentally observed energy levels. The dipole moments in the range 5.01–9.18 Debye validates the occurrence of charge transfer within the molecule. The large dipole moment (9.18 eV) in **4**, due to the presence of electron-withdrawing –NO_2 group increases the charge separation hence improving the charge transfer.

Table 3. Computed Ionization potentials, Electron affinities, Wavelengths, Oscillator strengths, main vertical electronic transition in the gas phase, Orbital energies, and Dipole moments of **1**–**4**.

Compd	E_a (eV)	I_p (eV)	I_{max} (nm)	F	Assignments	E_{HOMO} (eV)	E_{LUMO} (eV)	E_g(eV)	Dipole (debye)
1	1.25	7.53	404 345 311	0.0404 0.0906 0.0572	HOMO →LUMO (96 %) HOMO-1→LUMO (59%) HOMO−4 →LUMO+1(44%)	−6.18	−2.55	3.63	5.04
2	1.22	7.38	416 350 320	0.0337 0.0563 0.8341	HOMO →LUMO (97 %) HOMO −1 →LUMO (43%) HOMO →LUMO+1 (55%)	−6.05	−2.50	3.55	5.01
3	1.44	7.55	418 350 316	0.0310 0.0023 0.9085	HOMO →LUMO (97%) HOMO − 4→LUMO (92%) HOMO →LUMO +1(53%)	−6.25	−2.72	3.53	6.02
4	1.73	7.98	393 333 316	0.0681 0.3555 0.2474	HOMO →LUMO (91%) HOMO − 1→LUMO (60%) HOMO − 1→LUMO+ (32%)	−6.70	−2.99	3.71	9.18

The bandgap of molecules in the range 3.53–3.71 eV, exhibits a substitution effect. The small band gap in **2** (3.55 eV) and **3** (3.53 eV) could be attributed to electron-donating or + **I** effect of $-CH_3$ and +**M** effect of −Br substituent, in comparison to **1**. While strong electron-withdrawing/−**I** $-NO_2$ group responsible for larger bandgap in **4** (3.71 eV).

Finally, the optical properties were evaluated by TD–DFT in the gas phase, toluene, chloroform, and DMSO using the same parameters. The transitions above 350 nm correspond to inbuilt charge transfer in the dyes and were found to be affected by modulating peripheral electron-donating/withdrawing substituent. (See SI, **Table S5–S20**) Similar to experimentally observed absorption spectra, the computationally obtained λ_{max} are slightly sensitive towards solvent polarity (Toluene < $CHCl_3$ < DMSO. (see **SI, Figure S25**) The Cartesian coordinates of optimized structures, Mulliken and Lowdin charges of **1**–**4** given in SI **Table S1– S4**.

Thermal properties

The thermal stability of **1**–**4** was studied via thermogravimetric analysis (TGA) and the melting point was determined by the open capillary method. The TGA thermogram of **1**–**4** has been obtained in a nitrogen atmosphere at normal pressure with a heating rate of 10 °C/min and is displayed in **Figure 8**. The slight increase in mass on the heating cycle at beginning of the TGA thermogram can be attributed to the buoyancy effect [55].

TGA thermogram indicate that compounds **1**–**4** have good thermal stability. The decomposition temperature corresponds to 5% and 10% weight losses are found in the range 261–314 °C and 286–335 °C respectively (**Table 4**). The order of thermal stability in derivatives **1**–**4** is **4** > **3** > **2** > **1**.

Table 4. Thermal properties of compounds **1**–**4**.

Compound		1	2	3	4
TGA	$^{a}T_5$ (°C)	261	274	294	314
	$^{a}T_{10}$ (°C)	286	288	312	335

$^{a}T_5$ and T_{10} – temperature based on 5% and 10% weight loss from TGA curve

Conclusion

Indolo[2,3-*b*]quinoxalin-2-yl)(phenyl)methanone derivatives based on D–A architecture are synthesized through a simple cyclo condensation reaction. The inbuilt D-A architecture generates an ICT transition in the absorption spectrum of the molecule, which is noticeably influenced by electron-donating or withdrawing substituents present at the 9th position of indole moiety. Dyes emit blue–orange fluorescence (435–614 nm) on excitation at ICT maxima in toluene, ethyl acetate, chloroform, DMSO, and neat solid film. Emission maxima, ICT absorption band, and Stoke's shift of dyes reveal the existence of specific solute-solvent interaction.

The fluorescence study of dye **1** and **2** in different THF/water mixtures demonstrate the presence of AIEE in **1** and AIE in **2** with the formation of nano-aggregates, confirmed by DLS. Dyes exhibit low lying LUMO (–3.65 to –3.98 eV) which are comparable with reported n-type materials, display electron-transporting/injecting properties in **1**–**4**. Thermal properties reveal that the derivatives have a high melting point and good thermal stability. DFT and TD-DFT studies verify the inbuilt donor-acceptor architecture of **1**–**4**. The results indicate that synthesized compounds are potential candidates to be either used as n-type material or solid-state emitters in organic electronics.

Declarations

Acknowledgments

The authors are greatly thankful to Micro-Analytical Laboratory, Department of Chemistry, University of Mumbai for providing Instrumental facilities. We sincerely thank the Tata Institute of Fundamental Research

(TIFR), Mumbai for providing MALDI-TOF. One of the author DNK is grateful to DST-PURSE for JRF.

Authors Declarations

Funding

“The authors declare that no funds, grants, or other support were received during the preparation of this manuscript.”

Conflict of Interests

“The authors declared that there is no conflict of interest.”

Author Contribution

RK: Conceptualization, Investigation, Visualization, Supervision, Writing- Review and Editing. DK: Conception and design of work, data collection and analysis, data curation, investigation, Writing - Original draft. SD and AJ: contributed to data collection and analysis. MG and SC: Formal/Theoretical (computational) analysis.

Data Availability

All data generated or analysed during this study are included in this published article and its supplementary information files.

Code Availability

Not applicable

Ethics approval

Not applicable

Consent to participate

Not applicable

Consent to publish

Not applicable

References

1. Friend RH, Gymer RW, Holmes AB, Burroughes JH, Marks RN, Taliani C, Bradley DDC, Dos Santos DA, Brédas JL, Lögdlund M, Salaneck WR (1999) Electroluminescence in conjugated polymers. Nature 397:121–128. https://doi.org/10.1038/16393
2. Baldo MA, Thompson ME, Forrest SR (2000) High-efficiency fluorescent organic light emitting devices using a phosphorescent sensitizer. Nature 403:750–753. https://doi.org/10.1038/35001541

3. Anthony JE (2008) The larger acenes: versatile organic semiconductors. Angew Chem Int Ed 47:452–483. https://doi.org/10.1002/anie.200604045
4. Grätzel M (2009) Recent advances in sensitized mesoscopic solar cells. Acc Chem Res 42:1788–1798. https://doi.org/10.1021/ar900141y
5. Imahori H, Umeyama T, Ito S (2009) Large π-aromatic molecules as potential sensitizers for highly efficient dye-sensitized solar cells. Acc Chem Res 42:1809–1818. https://doi.org/10.1021/ar900034t
6. Ning Z, Tian H (2009) Triarylamine: a promising core unit for efficient photovoltaic materials. Chem Commun (Camb) 7:5483–5495. https://doi.org/10.1039/B908802D
7. Staub K, Levina GA, Barlow S, Kowalczyk TC, Lackritz HS, Fort A, Marder SR (2003) Synthesis and stability studies of conformationally locked 4-diarylaminoaryl- and 4-dialkylaminophenyl-substituted second-order nonlinear optical polyene chromophores. J Mater Chem 13:825–833. https://doi.org/10.1039/B208024A.
8. Jiao GS, Thoresen LH, Burgess K (2003) Fluorescent, through-bond energy transfer cassettes for labeling multiple biological molecules in one experiment. J Am Chem Soc 1226:14668–14669. https://doi.org/10.1021/ja037193l
9. Doré K, Dubus S, Ho HA, Lévesque I, Brunette M, Corbeil G, Boissinot M, Boivin G, Bergeron MG, Boudreau D, Leclerc M (2004) Fluorescent polymeric transducer for the rapid, simple, and specifc detection of nucleic acids at the zeptomole level. J Am Chem Soc 13:4240–4244. https://doi.org/10.1021/ja038900d
10. Luo J, Xie Z, Lam JWY, Cheng L, Chen H, Qiu C, Kwok HS, Zhan X, Liu Y, Zhu D, Tang BZ (2001) Aggregation-induced emission of 1-methyl-1,2,3,4,5-pentaphenylsilole. Chem Commun 18:1740–1741. https://doi.org/10.1039/B105159H
11. Yuan WZ, Lu P, Chen S, Lam JWY, Wang Z, Liu Y, Kwok HS, Ma Y, Tang BZ (2010) Changing the Behavior of Chromophores from Aggregation–Caused Quenching to Aggregation-Induced Emission: Development of Highly Efficient Light Emitters in the Solid State. Adv Mater 22:2159–2163. https://doi.org/10.1002/adma.200904056
12. Mei J, Leung NLC, Kwok RTK, Lam JWY, Tang BZ (2015) Aggregation-Induced Emission: Together We Shine, United We Soar! Chem Rev 115: 11718–11940. https://doi.org/10.1021/acs.chemrev.5b00263
13. Zhang W, Yu G (2015) Organic optoelectronics materials, Springer, Switzerland, 60-61. https://doi.org/10.1007/978-3-319-16862-3
14. Zhang W, Yu G (2015) Organic optoelectronics materials, Springer, Switzerland, 67–75. https://doi.org/10.1007/978-3-319-16862-3
15. Quinn JTE., Zhu J, Li X, Wangb J, Li Y (2017) Recent progress in the development of n-type organic semiconductors for organic field effect transistors J Mater Chem C 5:8654–8681. https://doi.org/10.1039/C7TC01680H
16. Winkler M, Houk KN (2007) Nitrogen-rich oligoacene's: candidates for n-channel organic semiconductor. J Am Chem Soc 129:1805–1815. https://doi.org/10.1021/ja067087u
17. Shaikh AM, Sharma BK, Chacko S, Kamble RM (2016) Synthesis and optoelectronic investigations of triarylamines based on naphtho[2,3-*f*]quinoxaline-7,12-dione core as donor-acceptors for n-type

materials. RSC Adv 6:60084–60093. https://doi.org/10.1039/C6RA11149A

18. Shaikh AM, Sharma BK, Kamble RM (2015) Synthesis, photophysical, electrochemical and thermal studies of triarylamines based on benzo[*g*]quinoxalines. J Chem Sci 127:1571–1579. https://doi.org/10.1007/s12039-015-0904-0.
19. Kanekar DN, Chacko S, Kamble RM (2019) Quinoxaline based amines as Blue-orange emitters: effect of modulating donor system on Optoelectrochemical and theoretical properties. Dyes Pigm 167:36–50. https://doi.org/10.1016/ j.dyepig.2019.04.005.
20. Mahadik SS, Chacko S, Kamble RM (2019) 2,3-Di(thiophen-2-yl)quinoxaline amine derivatives: yellow-blue fluorescent materials for applications in organic electronics. ChemistrySelect 4:10021–10032. https://doi.org/10.1002/ slct.201902109.
21. Singh PS, Chacko S, Kamble RM (2019) The design and synthesis of 2,3-diphenylquinoxaline amine derivatives as yellow-blue emissive materials for optoelectrochemical study. New J Chem 43:6973–6988. https://doi.org/ 10.1039/C9NJ00248K.
22. Sharma BK, Shaikh AM, Chacko S, Kamble RM (2017) Synthesis, Spectral, Electrochemical and Theoretical Investigation of indolo[2,3-*b*]quinoxaline dyes derived from Anthraquinone for n–type materials. J Chem Sci 129:483–494. DOI 10.1007/s12039-017-1252-z
23. Singh PS, Badani PM, Kamble RM (2019) Impact of the donor substituent on the optoelectrochemical properties of 6*H*-indolo[2,3-*b*]quinoxaline amine derivatives. New J Chem 43:19379-19396. https://doi.org/10.1039/ c9nj05558d.
24. Shaikh AM, Sharma BK, Chacko S, Kamble RM (2016) Synthesis and opto-electrochemical properties of tribenzo[*a,c,i*]phenazine derivatives for hole transport materials. RSC Adv 6:94218–94227. https://doi.org/10.1039/ C6RA20964E.
25. Shaikh AM, Sharma BK, Chacko S, Kamble RM (2017) Novel electroluminescent donor–acceptors based on dibenzo[*a*,*c*]phenazine as hole-transporting materials for organic electronics. New J Chem 41:628–638. DOI: 10.1039/c6nj03553a.
26. Kanekar DN, Chacko S, Kamble RM (2020) Synthesis and investigation of the photophysical, electrochemical and theoretical properties of phenazine–amine based cyan blue-red fluorescent materials for organic electronics. New J Chem 44:3278–3293. https://doi.org/10.1039/c9nj06109f.
27. Mahadik SS, Garud DR, Ware AP, Pingale SS, Kamble RM (2021) Design, Synthesis and Opto-electrochemical Properties of Novel 2,3-di(hetero-2-yl)pyrido[2,3-*b*]pyrazine amine derivatives as Blue-Orange Fluorescent Materials. Dyes Pigm 184:108742. doi:10.1016/j.dyepig.2020.108742.
28. Singh PS, Ghadiyali M, Chacko S, Kamble RM (2022) D–A–D based pyrido-pyrazino[2,3-*b*]indole amines as blue-red fluorescent dyes: Photophysical, aggregation-induced emission, electrochemical and theoretical studies. J Lumin 242:118568. https://doi.org/10.1016/j.jlumin.2021.118568
29. Kanekar DN, Chacko S, Kamble RM (2018) Synthesis, opto-electrochemical and theoretical investigation of pyrazino[2,3-*b*]phenazine amines for organic electronics. ChemistrySelect 3:4114–4123. https://doi.org/10.1002/ slct.201800562.
30. Sharma BK, Shaikh AM, Agarwal N, Kamble RM (2016) Synthesis, photophysical and electrochemical studies of acridone-amine based donor–acceptors for hole transport materials. RSC Adv 6:17129–

17137. DOI: 10.1039/c5ra25115j

31. Shaikh AM, Chacko S, Kamble RM (2017) Synthesis, Optoelectronic and Theoretical Investigation of Anthraquinone Amine-Based Donor-Acceptor Derivatives. ChemistrySelect 2: 7620– 7629. DOI: 10.1002/slct.201701475
32. Harmenberg J, Wahren B, Bergman J, Akerfeldt S, Lundlad L (1988) Antiherpesvirus activity and mechanism of action of indolo-[2,3-*b*]quinoxaline and analogs. Antimicrob Agents Chemother 32:1720–1724. DOI: 10.1128/aac.32.11.1720
33. Harmenberg J, Akesson-Johansson A, Gräslund A, Malmfors T, Bergman J, Wahren B, Akerfeldt S et al (1991) The mechanism of action of the anti-herpes virus compound 2,3-dimethyl-6(2-dimethylaminoethyl)-6*H*-indolo-[2,3-*b*]quinoxaline. Antiviral Res 15:193-204. DOI: 10.1016/0166-3542(91)90066-z
34. Hirata K, Araya J, Nakaike S, Kitamura K, Ishida T (2001) Side chain-dependent binding of antitumor indoloquinoxaline derivatives to DNA: comparative spectroscopic and viscometric measurements. Chem Pharm Bull 49:44—48. DOI: 10.1248/cpb.49.44.
35. Deady LW, Kaye AJ, Finlay GJ, Baguley BC, Denny WA (1997) Synthesis and antitumor properties of N-[2-(dimethylamino)ethyl]carboxamide derivatives of fused tetracyclic quinolines and quinoxalines: a new class of putative topoisomerase inhibitors. J Med Chem 40:2040—2046. doi: 10.1021/jm970044r.
36. Manna K, Agrawal YK (2009) Microwave assisted synthesis of new indophenazine 1,3,5-trisubstruted pyrazoline derivatives of benzofuran and their antimicrobial activity. Bioorg Med Chem Lett 19:2688—2692. DOI: 10.1016/j.bmcl.2009.03.161.
37. Pai NR, Pusalkar DA (2010). Pharmacological screening of novel indolo[2,3-*b*]quinoxaline derivatives. J Chem Pharm Res 2:485–493. ISSN:0975-7384
38. Sharma V, Kumar P, Pathaka D (2010) Biological Importance of the Indole Nucleus in Recent Years: A Comprehensive Review. J Heterocycl Chem 47:491–502. DOI 10.1002/jhet
39. Slater LS, Callis PR (1995) Molecular Orbital Theory of the 1La and $1L_b$ States of Indole. 2. An ab Initio Study. J Phys Chem 99:8572–8581. 10.1021/j100021a020
40. Jennings P, Jones AC, Mount AR (1998) Fluorescence properties of electropolymerised 5-substituted indoles in solution. J Chem Soc, Faraday Trans 94: 3619–3624. https://doi.org/10.1039/A806721J
41. Walker MS, Bednar TW, Lumry R (1967) Exciplex Studies. II. Indole and Indole Derivatives. **J Chem Phys** 47:1020–1028. https://doi.org/10.1063/1.1711983
42. Beauchard A, Ferandin Y, Frere S, Lozach O, Blairvacq M, Meijer L, Thiery V, Besson T (2006) Synthesis of novel 5-substituted indirubins as protein kinases inhibitors Bioorg Med Chem 14:6434-43. DOI: 10.1016/j.bmc.2006.05.036
43. Bergman J, Charlotta D (1996) Synthesis of pyridopyrazino[2,3-*b*] indoles and 10*H*-indolo[3,2-*g*]pteridins. Recl Trav Chim Pays-Basb 115:31—36. https://doi.org/10.1002/recl.19961150107
44. Martinaud M, Kadiri A (1978) Comparative sensibility of S1←S0 and S2←S0 indole electronic transitions to environment perturbations. The positions of the 0—0 bands in polar media. Chem Phys 28:473-485. 10.1016/0301-0104(78)80026-3

45. Lakowicz JR (2006) Solvent and environmental effects. In: Lakowicz JR. (eds) Principles of fluorescence spectroscopy. Boston, MA: Springer. https://doi.org/10.1007/978-0-387-46312-4
46. Zhu X, Su Q, Feng W, Li F (2017) Anti-Stoke's shift luminescent materials for bio-applications Chem Soc Rev 46:1025–1039. https://doi.org/10.1039/C6CS00415F
47. Kasai H, Nalwa HS, Oikawa H, Okada S, Matsuda H, Minami N, Kakuta A, Ono K, Mukoh A, Nakanishi H (1992) A novel preparation method of organic microcrystals. Jpn J Appl Phys 31:L1132–L1134. https://doi: org/10.1143/JJAP.31.L1132
48. Yang W, Li C, Zhang M, Zhou W, Xue R, Liu H, Li Y (2016) Aggregation-induced emission and intermolecular charge transfer effect in triphenylamine fluorophores containing diphenylhydrazone structures. Phys Chem Chem Phys 18:28052–60. https://doi.org/10.1039/C6CP04755F
49. Liu W, Ying S, Zhang Q, Ye S, Guo R, Ma D, Wang L (2018) New multifunctional aggregation-induced emission fuorophores for reversible piezofuorochromic and nondoped sky-blue organic light-emitting diodes. Dyes Pigm 158:204–212. https://doi.org/10.1016/j.dyepig.2018.05.030
50. Li H, Chi Z, Zhang X, Xu B, Liu S, Zhang Y, Xu J (2011) New thermally stable aggregation-induced emission enhancement compounds for non-doped red organic light-emitting diodes. Chem Commun 47:11273–11275. https://doi.org/10.1039/C1CC14642D
51. Chikamatsu M, Itakura A, Yoshida Y, Azumi R, Yase K (2008) High-performance n-type organic thin-film transistors based on solution-processable perfuoroalkyl-substituted C60 derivatives. Chem Mater 20:7365–7367. https://doi.org/10.1021/cm802577u
52. Byung B, Jung J, Lee K, Sun J, Andreou AG, Katz HE (2010) Air-operable, high-mobility organic transistors with semi-fluorinated side chains and unsubstituted naphthalenetetracarboxylic diimide cores: high mobility and environmental and bias stress stability from the perfluorooctylpropyl side Chain. Adv Funct Mater 20:2930–2944. https://doi.org/10.1002/adfm.201000655
53. Q. Zheng, J. Huang, A. Sarjeant, H. E. Katz, (2008) Pyromellitic Diimides: Minimal Cores for High Mobility n-Channel Transistor Semiconductors. J Am Chem Soc 130:14410–14411. https://doi.org/10.1021/ja805746h
54. Frisch MJ, Trucks GW, Schlegel HB, Scuseria GE, Robb MA, Cheeseman JR, Montgomery JA Jr, Vreven T, Kudin KN, Burant JC, Millam JM, Iyengar SS, Tomasi J, Barone V, Mennucci B, Cossi M, Scalmani G, Rega N, Petersson GA, Nakatsuji H, Hada M, Ehara M, Toyota K, Fukuda R, Hasegawa J, Ishida M, Nakajima T, Honda Y, Kitao O, Nakai H, Klene M, Li X, Knox JE, Hratchian HP, Cross JB, Bakken V, Adamo C, Jaramillo J, Gomperts R, Stratmann RE, Yazyev O, Austin AJ, Cammi R, Pomelli C, Ochterski JW, Ayala PY, Morokuma K, Voth GA, Salvador P, Dannenberg JJ, Zakrzewski VG, Dapprich S, Daniels AD, Strain MC, Farkas O, Malick DK, Rabuck AD, Raghavachari K, Foresman JB, Ortiz JV, Cui Q, Baboul AG, Cliford S, Cioslowski J, Stefanov BB, Liu G, Liashenko A, Piskorz P, Komaromi I, Martin RL, Fox DJ, Keith T, Al-Laham MA, Peng CY, Nanayakkara A, Challacombe M, Gill PMW, Johnson B, Chen W, Wong MW, Gonzalez C, Pople JA (2004) Gaussian, 03, Revision C02. Gaussian Inc, Wallingford CT.
55. Bottom R (2008) Thermogravimetric analysis. In: Gabbott P (ed) Principles and applications of thermal analysis wiley online books, pp 87–118. https://doi.org/10.1002/9780470697702.ch3

Scheme

Please see the Supplementary Files for the Scheme 1.

Figures

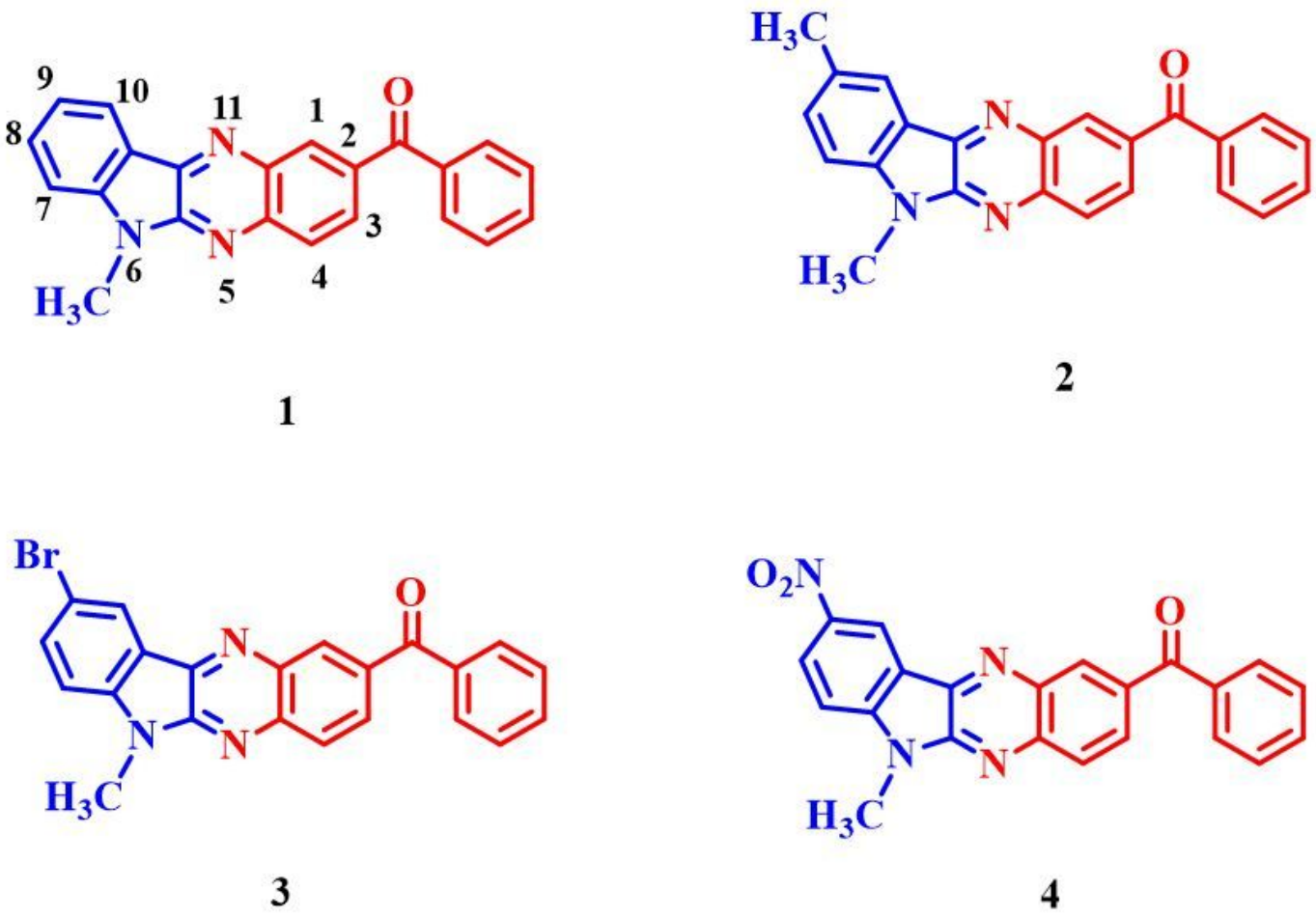

Figure 1

Synthesized indolo[2,3-*b*]quinoxalin-2-yl)(phenyl)methanone derivatives **1**–**4**.

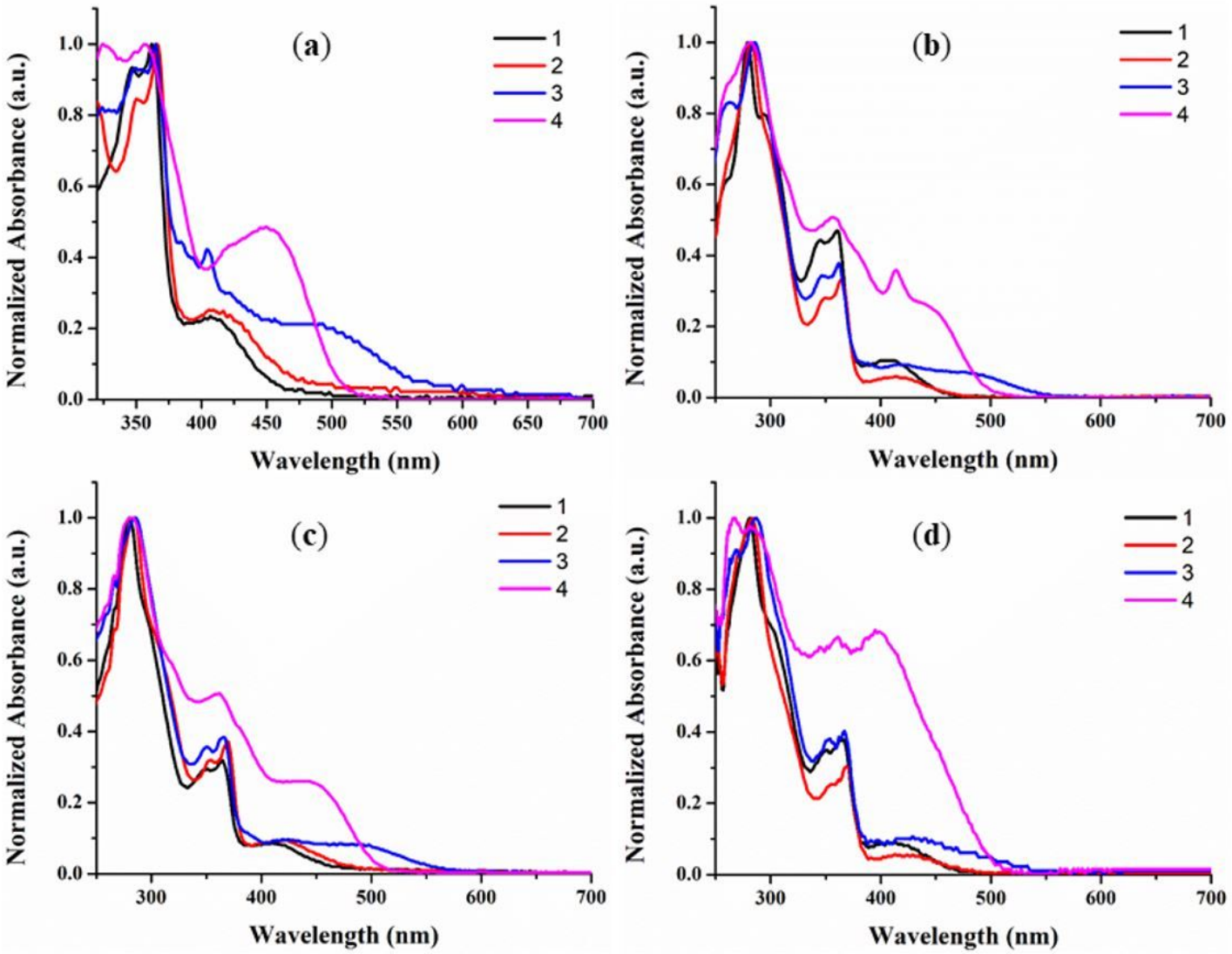

Figure 2

Absorption spectra of compounds **1**–**4** in toluene (**a**), Ethyl acetate (**b**), chloroform (**c**), and dimethyl sulphoxide (**d**).

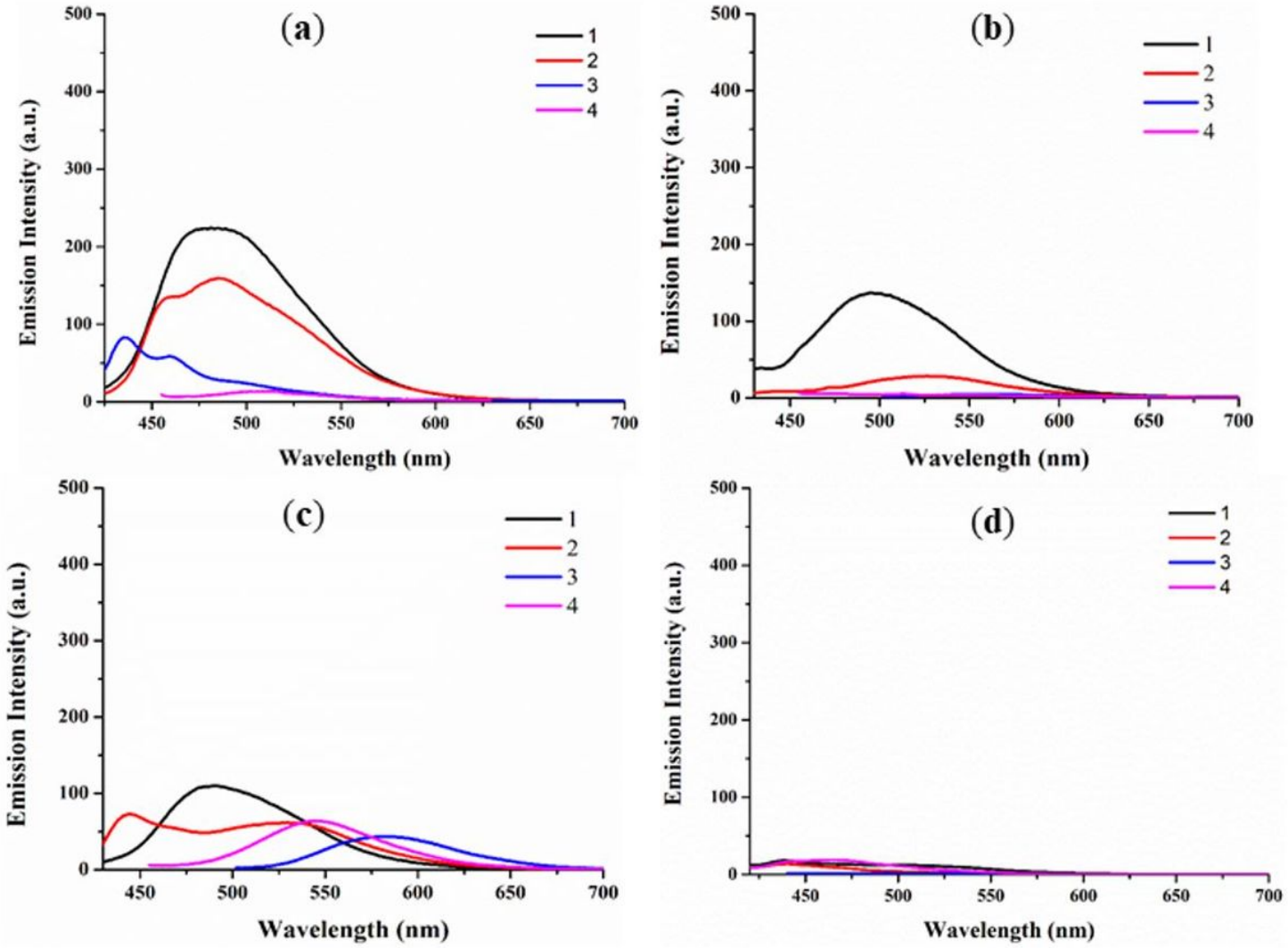

Figure 3

Emission spectra of compounds **1**–**4** in toluene (**a**), Ethyl acetate (**b**), chloroform (**c**), and dimethyl sulphoxide (**d**).

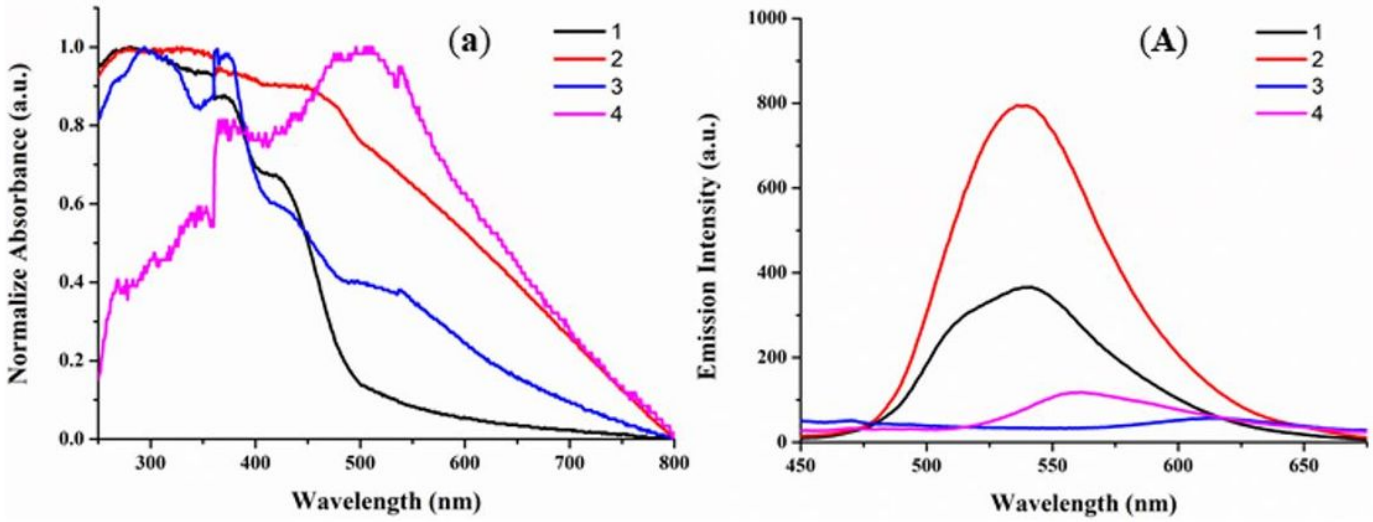

Figure 4

Absorption spectra (**a**) and Emission spectra (**A**) of **1**–**4** in a neat solid film.

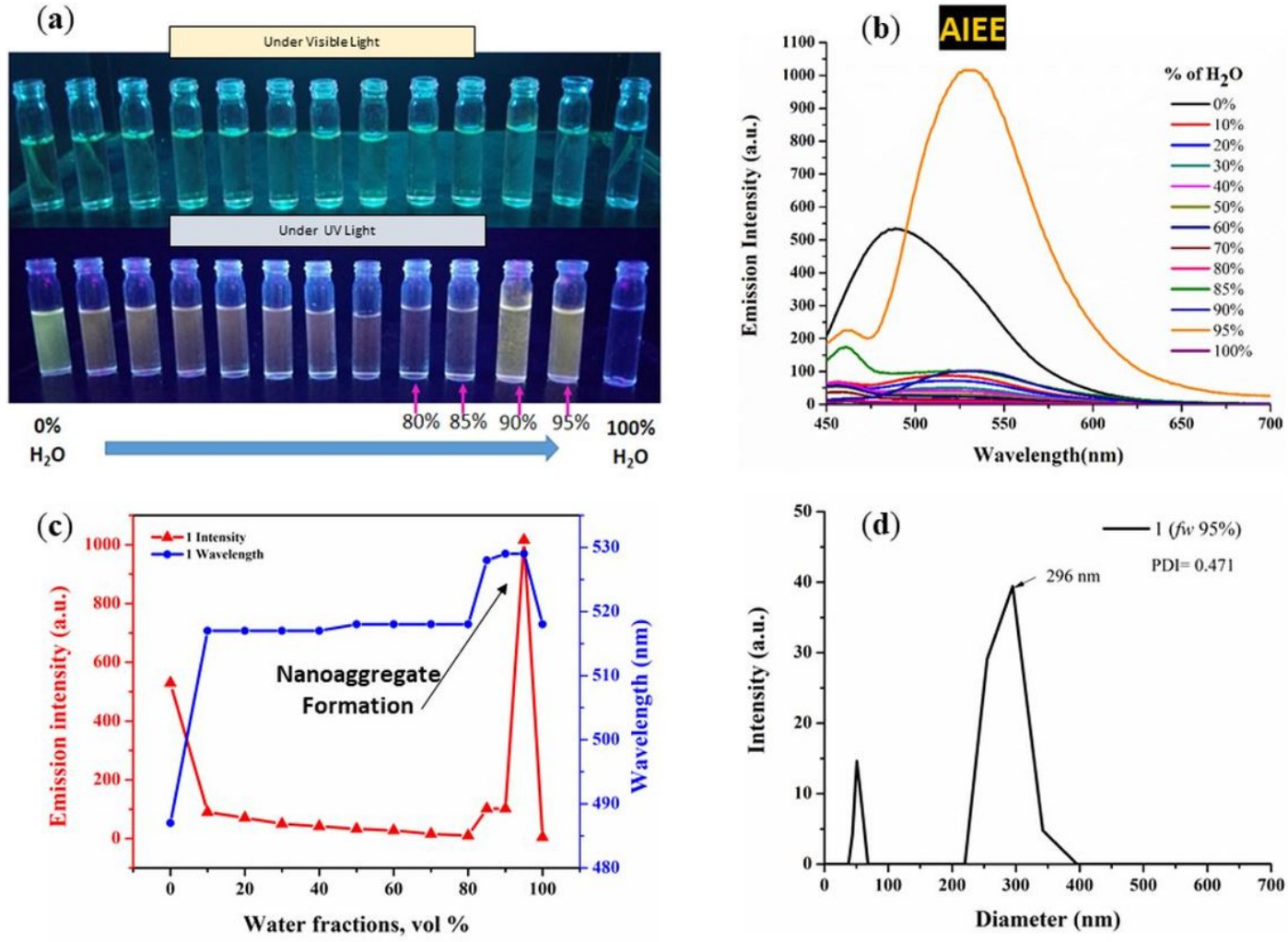

Figure 5

Fluorescence image of **1** in THF–water mixture with subsequently increasing water fractions (10^{-5} M) by 10% up to 80% and by 5% from 80% to 100% under UV–Visible light (**a**); Fluorescence spectra of **1** in THF–water mixture (10^{-5} M) with increasing water fractions (f_w) (**b**); plots of PL intensity and peak wavelength versus f_w (**c**) and DLS plot of **1** obtained for nano-aggregates formed in f_w = 95% of THF–water mixture (**d**).

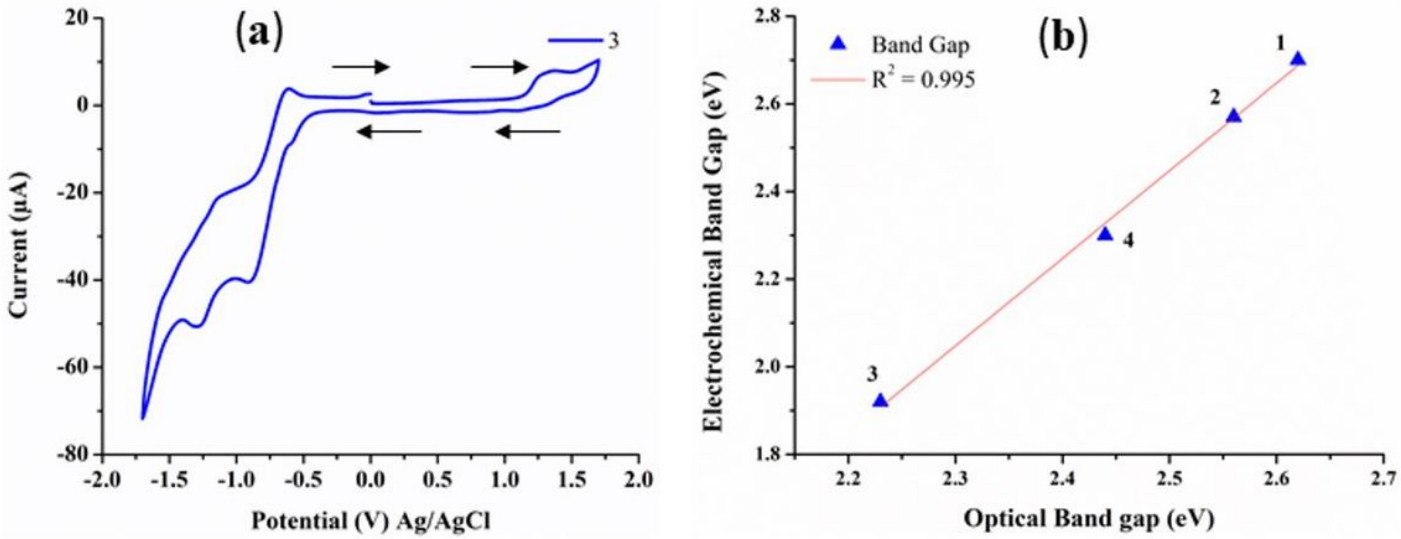

Figure 6

Cyclic voltammogram (full scan) of dye **3** (**a**) in anhydrous dichloromethane and graph of optical vs electrochemical bandgap (**b**).

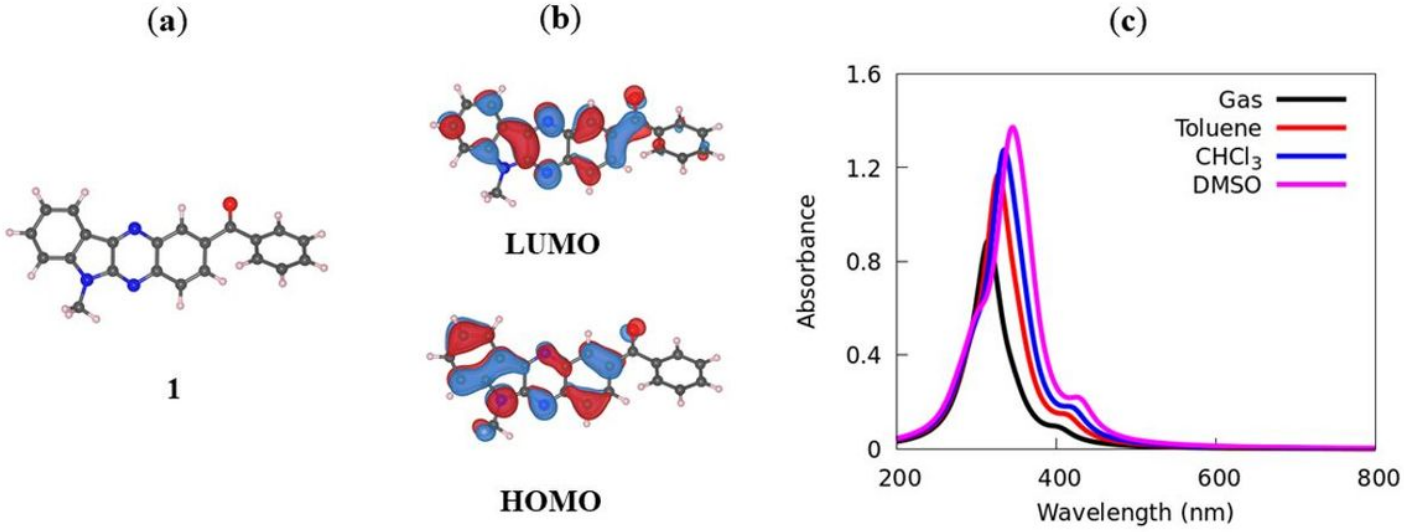

Figure 7

Optimized structure (**a**) and Frontier molecular orbitals (**b**) of **1** in the gas phase; and simulated absorption spectra of **1** in gas, toluene, $CHCl_{3,}$ and DMSO.

Figure 8

TGA thermogram of **1**–**4** under nitrogen atmosphere at normal pressure. Heating rate, 10 $^{\circ}$C/min.

Supplementary Files

This is a list of supplementary files associated with this preprint. Click to download.

- graphicsabstract.jpg
- scheme1.jpg
- SupportingInformation.docx